Structural Analysis Identifies Imidazo[1,2-*b*]Pyridazines as PIM Kinase Inhibitors with *In vitro* Antileukemic Activity

Vanda Pogacic,[1] Alex N. Bullock,[2] Oleg Fedorov,[2] Panagis Filippakopoulos,[2] Christelle Gasser,[1] Andrea Biondi,[3] Sandrine Meyer-Monard,[1] Stefan Knapp,[2] and Juerg Schwaller[1]

[1]University Hospital Basel, Department of Research and the Hematology Clinic, Basel, Switzerland; [2]Oxford University, Structural Genomics Consortium, Botnar Research Centre, Oxford, United Kingdom; and [3]Centro M. Tettamanti-Clinica Pediatrica Universita Milano-Bicocca, Monza, Italy

Abstract

Much attention has recently been focused on PIM kinases as potential targets for the treatment of hematopoietic malignancies and some solid cancers. Using protein stability shift assays, we identified a family of imidazo[1,2-*b*]pyridazines to specifically interact with and inhibit PIM kinases with low nanomolar potency. The high-resolution crystal structure of a PIM1 inhibitor complex revealed that imidazo[1,2-*b*]pyridazines surprisingly interact with the NH_2-terminal lobe helix αC rather than with the kinase hinge region. Thus, the identified inhibitors are ATP competitive but not ATP mimetic compounds, explaining their enhanced selectivity with respect to conventional type I kinase inhibitors. One of the identified imidazo[1,2-*b*]pyridazines (K00135) was further tested in several hematopoietic cellular systems. First, K00135 dose-dependently impaired survival of murine Ba/F3 cells that have been rendered cytokine independent by overexpression of human PIMs. Second, K00135 impaired survival and clonogenic growth of a panel of human acute leukemia cells. Third, exposure of K00135 significantly suppressed *in vitro* growth of leukemic blasts from five acute myelogenous leukemia patients but not of normal umbilical cord blood mononuclear cells. *In vitro* kinase assays and immunoblotting using lysates from human MV4;11 leukemic cells showed inhibition of phosphorylation of known PIM downstream targets, such as BAD and eukaryotic translation initiation factor 4E–binding protein 1, by K00135. Taken together, we report a family of small molecules that selectively interact and block PIM kinases and could serve as a lead to develop new targeted antileukemic therapeutics. [Cancer Res 2007;67(14):6916–24]

Introduction

Genetic alterations leading to uncontrolled protein tyrosine kinase activity are a hallmark of myeloproliferative disorders. Fusion genes involving ABL or platelet-derived growth factor receptor are the molecular correlate of chronic myeloid leukemia, whereas activating mutations of FLT3 or KIT are recurrently found in human acute myelogenous leukemia (AML; refs. 1, 2). The success of small molecules that block oncogenic tyrosine kinase activity, like imatinib-mesylate (Gleevc, Novartis), provided a proof of principle for targeted antileukemic therapy (3). However, the successful clinical use of such specific inhibitors has been challenged by the development of drug resistance and a limited clinical efficacy in patients with acute leukemia (4). To overcome these limitations, identification of critical signaling mediators downstream of an oncogenic tyrosine kinase is essential to delineate new targets that would allow development of an efficient combined therapeutic approach. Strong evidence exists that most oncogenic tyrosine kinases mediate malignant transformation by *parallel* activation of several signaling pathways such as Janus-activated kinase/signal transducers and activators of transcription (STAT), phosphatidylinositol 3-kinase/Akt, Ras/Raf/mitogen-activated protein kinase, or nuclear factor κB (1, 2).

Retroviral gene tagging in *c-myc*–induced murine lymphomas led to identification of the PIM serine/threonine kinase family that, in humans, encompasses three members: PIM1, PIM2, and PIM3 (5, 6). PIM1 has been characterized as one of the first target genes of STAT5 (7, 8). Several groups have shown that constitutive STAT5 activation is a hallmark of a wide spectrum of hematologic malignancies and that STAT5 is an essential mediator for transformation by oncogenic tyrosine kinases (9, 10). Interestingly, PIM1 and PIM2 have been found to be overexpressed in leukemia and lymphoma (11–13). Further *in vitro* functional studies have provided evidence that activation of PIM1 and/or PIM2 is important for malignant transformation by oncogenic tyrosine kinases such as FLT3 internal tandem duplications (FLT3-ITD), expressed in ~25% of human AML cases (12, 14–17). These studies suggested that small molecules inhibiting PIM kinases could provide a promising therapeutic avenue for hematologic malignancies.

To facilitate development of lead compounds, several groups have reported the crystal structure of PIM1 in complex with a number of ATP mimetic kinase inhibitors with broad kinase inhibition profile (18–22). The crystal structures of PIM1 and PIM2 (pdb code 2IWI)[4] showed that PIM kinases have an atypical hinge region characterized by an insertion of one additional residue and the presence of a proline that allows formation of only one hydrogen bond with ATP or ATP mimetic inhibitors. Despite this unique structural feature, all inhibitors published to date interact with the kinase hinge region in a classic ATP mimetic way (18–22).

Here, we report imidazo[1,2-*b*]pyridazines as inhibitors of PIM kinases. Despite high sequence homology and conservation of the active site, the identified inhibitors were on average 100-fold

Note: Supplementary data for this article are available at Cancer Research Online (http://cancerres.aacrjournals.org/).

Requests for reprints: Juerg Schwaller, Department of Research, University Hospital Basel, Hebelstrasse 20, CH-4031 Basel, Switzerland. Phone: 41-61-265-3504; Fax: 41-61-265-2350; E-mail: J.Schwaller@unibas.ch or Stefan Knapp, Structural Genomics Consortium, Botnar Research Centre, Oxford University, Oxford OX3 7LD, United Kingdom. Phone: 44-1-865-227978; Fax: 44-1-865-737231; E-mail: stefan.knapp@sgc.ox.ac.uk.

doi:10.1158/0008-5472.CAN-07-0320

[4] Unpublished data.

selective for PIM1 over PIM2. The selected lead compounds were highly selective and cross-reacted only with one additional kinase (Cdc-like kinase 1) when screened against a panel of 50 kinase catalytic domains. Determination of the cocrystal structure with K00135 suggested that the unusual binding mode of the studied inhibitor is responsible for the enhanced selectivity of this scaffold. In addition, we show that this inhibitor has *in vitro* antileukemic potential as shown in various cell line models as well as primary AML patient samples.

Materials and Methods

Protein expression and purification. Full-length human *PIM1* (gi|33304198) was subcloned and protein was expressed and purified as previously described (21). The masses of purified proteins were confirmed by liquid chromatography-mass spectrometry using an Agilent LC/MSD TOF system with reversed-phase high-performance liquid chromatography coupled to electrospray ionization and an orthogonal time-of-flight mass analyzer. The purified PIM1 protein was homogeneous and had an experimental mass of 35,546 Da as expected from its primary structure.

Kinase assay. Phosphorylation reactions were monitored using a coupled-enzyme assay in which ADP production was coupled to NADH oxidation by pyruvate kinase and lactate dehydrogenase (23). The assay was carried out in 100 μL of a buffer containing 50 mmol/L HEPES (pH 7.5), 100 mmol/L NaCl, 10 mmol/L $MgCl_2$, 1 mmol/L phosphoenolpyruvate, 0.1 mmol/L NADH, 30 μg/mL pyruvate kinase, 10 μg/mL lactate dehydrogenase, and either 20 nmol/L PIM1 or PIM2. The reaction was monitored at 340 nm at 25°C on a Spectramax spectrophotometer (Molecular Devices) and started by addition of 100 μmol/L ATP after a 10-min preincubation at 25°C. A recognition peptide of the PIM1 substrate p21 (RKRRQTSMTD) was used at 30 μmol/L. DMSO-dissolved inhibitors were added at the preincubation period resulting in a 2% final DMSO. Kinetic analysis was done by nonlinear regression fitting using the program KaleidaGraph (Synergy Software).

Protein stability shift assay. Thermal melting experiments were carried out using the Mx3005p real-time PCR machine (Stratagene). Proteins (2 μmol/L, final) were assayed in 10 μL of 10 mmol/L HEPES (pH 7.5), 150 mmol/L NaCl in a 96-well plate. Inhibitors were added at a final concentration of 10 μmol/L. SYPRO Orange (Molecular Probes; dilution, 1:1,000) was added as a fluorescence probe. Excitation and emission filters for the SYPRO-Orange dye were set at 465 and 590 nm, respectively. The temperature was raised at 1°C/min from 25°C to 96°C and fluorescence readings were taken at each interval. The temperature dependence of the fluorescence during the protein denaturation process was approximated by the equation

$$y(T) = y_F + \frac{y_U - y_F}{1 + e^{\Delta uG_{(T)}/RT}}$$

where ΔuG is the difference in unfolding free energy between the folded and unfolded state, R is the gas constant, and y_F and y_U are the fluorescence intensity of the probe in the presence of completely folded and unfolded protein, respectively (24). The baselines of the denatured and native state were approximated by a linear fit. The observed temperature shifts, ΔT_m^{obs}, for each inhibitor were recorded as the difference between the transition midpoints of sample and reference wells containing protein without inhibitor in the same plate and determined by nonlinear least squares fit. All compounds were purchased from BioFocus.

Crystallization. Nonphosphorylated PIM1 sample was concentrated (final, 10 mg/mL) in the presence of ligands 0.7 mmol/L "pimtide" (ARKRRRHPSGPPTA-amide) and 1 mmol/L imidazopyridazine inhibitor. Crystals were grown in a sitting drop setup at 4°C by mixing 100 nL of this sample with 50 nL of precipitant [40% polyethylene glycol 300, 0.1 mol/L Tris (pH 8.5), 0.2 mol/L Li_2SO_4]. The imidazopyridazine inhibitor [1-(3-{6-[(cyclopropylmethyl)amino]imidazo[1,2-*b*]pyridazin-3-yl}phenyl) ethanone; referred as K00135] was purchased from BioFocus and added to a final 1 mmol/L from a 50 mmol/L stock in DMSO.

Structure determination. PIM1 diffraction data were collected on a cryofrozen crystal (100K) at the Swiss Light Source synchrotron beam line SLS-X10. Images were indexed and integrated using MOSFLM (25) and scaled using SCALA (26) implemented in the CCP4 (CCP4, 1994) suite of programs. The structure was solved using molecular replacement and the program Phaser (27) using the PIM1 in a complex with the bisindolyl maleide inhibitor BIM1 as a search model. Both structures were refined with REFMAC5 (28) using iterative rounds of rigid-body and restrained refinement with translation-libration-screw against maximum likelihood targets, interspersed with manual rebuilding of the model using Xfit/XtalView (29).

Coordinates. Coordinates have been deposited in the Protein Data Bank (pdb accession code 2C3I).

Reagents. Anti–phospho-BAD (Ser^{112}), anti–phospho-BAD (Ser^{136}), anti-BAD, anti–phospho-eukaryotic translation initiation factor 4E–binding protein 1 (4E-BP1; $Thr^{37/46}$), and anti–phospho-4E-BP1 (Thr^{70}) rabbit polyclonal antibodies were purchased from Cell Signaling Technology. Anti-FLAG (clone M2) mouse monoclonal antibody (mAb) was obtained from Sigma-Aldrich. Anti-actin antibody and anti-PIM1 mouse mAb were from Santa Cruz Biotechnology and anti-PIM2 rabbit polyclonal antibody was from Abgent. Z-Leu-Leu-Leu-al (MG132) was purchased from Sigma-Aldrich.

Generation of stable cell lines expressing human PIM1/PIM2 and inhibitor treatment. The murine interleukin-3 (IL-3)–dependent hematopoietic cell line Ba/F3 was maintained in RPMI 1640 containing 10% FCS and 1 ng/mL recombinant murine IL-3 (PeproTech EC). The cDNAs encoding human *PIM1* and *PIM2* were reverse transcription-PCR (RT-PCR) amplified (with or without a FLAG tag) from mRNA extracted from human leukemic cell line K562 and cloned into *Eco*RI/*Xho*I sites of pMSCV-IRES-EYFP (PIM1) and into *Bgl*II/*Eco*RI sites of pMSCV-IRES-EGFP (PIM2). High-titer retroviral supernatants were produced as previously described (17). Transduced Ba/F3 cells were selected for IL-3–independent growth. Expression of FLAG-tagged PIM1/PIM2 was verified by real-time RT-PCR and Western blotting (on treatment with 10 μmol/L MG123 for various amounts of time). Cellular growth curves were established by daily counting of the cultures at a starting density of 10^5 cells/mL. To investigate the effect on the cell proliferation, K00135 (dissolved in DMSO) was added to the culture medium (0.1, 1, and 10 μmol/L) and 0.1% DMSO was added to the control cultures. Cell viability was analyzed by trypan blue dye exclusion and normalized as percentage to control cultures after 24 h.

Human cell lines and treatment with PIM inhibitor. Human leukemia cell lines MV4;11, RS4;11, MOLM13, KOCL45, SEM, KOPN8, and K562 were purchased from DSMZ and maintained in RPMI 1640 with 10% FCS and 1% penicillin-streptomycin at 37°C in 5% CO_2. To investigate the effect on the cell proliferation, either K00135 (in DMSO, 0.1, 1, 10 μmol/L final) or 0.1% DMSO was added to the culture medium and the cultures were incubated for 48 h (1×10^5 cells in 1 mL). Cell proliferation and viability were assayed using 200 μL of the initial culture and Cell Proliferation Reagent WST-1 from Roche Diagnostics according to the manufacturer's instructions. Cell survival was calculated as a percentage normalized to control cultures and IC_{50} values were calculated using Forecast function of Excel.

Primary AML samples. Peripheral blood samples were collected with informed consent from patients with newly diagnosed or recurrent AML. Mononuclear cells were separated by Ficoll-Histopaque and frozen in 10% DMSO. Cells were then either used for colony formation assays, as described below, or cultured in AIM-V medium (Cambrex) supplemented with 10% FCS, 1 mmol/L L-glutamine, and 1% penicillin-streptomycin. Cord blood was isolated from healthy donors under informed consent, and mononuclear cells were separated by Ficoll-Histopaque gradient and used as a control for compound-related cytotoxicity. To investigate the effect on cell proliferation, either K00135 (in DMSO, 1, 5, 10 μmol/L final) or 0.1% DMSO was added to the culture (1×10^5 living cells/mL in 2 mL) and cell viability analyzed by trypan blue dye exclusion after 24 h.

***In vitro* colony forming assay.** Cells (10^4) were plated in methylcellulose (2 mL; MethoCult SF^{BIT} H4236, StemCell Technologies) supplemented

with 10% FCS and either K00135 (1 or 4 μmol/L) or DMSO (0.1%) alone, and grown in 35-mm Petri dishes in a humidified atmosphere with 5% CO_2 at 37°C. Light microscopy was done 8 days later to assess colony formation (a colony was defined as a cluster of ≥50 cells). Mononuclear blood cells (5×10^5) from the AML patients were plated in "complete" methylcellulose (2 mL; MethoCult GF H4534, StemCell Technologies) supplemented with either K00135 (1, 5, and 10 μmol/L) or 1% DMSO alone and grown as above. All cultures were inspected 10 days later for leukemic cell growth and pictures were taken.

Analysis of apoptosis. MV4;11 cells were treated with 1 μmol/L K00135 for 48 h and analyzed at various time points by flow cytometry using both violet fluorescent dye PO-PRO-1 (a sensitive indicator of apoptotic cells) and 7-amino-actinomycin D (indicator of dead cells) from the Vybrant Apoptosis Assay Kit #13 (Molecular Probes) according to the manufacturer's instructions.

Protein extraction and Western blotting. MV4;11 cells were grown at 3×10^5/mL to 5×10^5/mL, treated with 1 to 3 μmol/L K00135 for various times, harvested, and rinsed with ice-cold PBS. Ice-cold lysis buffer [10 mmol/L Tris-HCl (pH 7.4), 150 mmol/L NaCl, 1% Triton X-100, 0.5 mmol/L EDTA, 10% glycerol, 10 mmol/L NaF, 1 mmol/L Na_3VO_4, protease inhibitor cocktail] was added to the cells and incubated on ice for 20 min followed by 5-min microcentrifugation. Proteins were precipitated from supernatant using methanol-chloroform, and then pellets were resuspended in Laemmli's sample buffer, separated by SDS-PAGE, and transferred to the membranes. The membranes were blotted with primary antibodies (diluted according to the manufacturer's recommendations), followed by horseradish peroxidase–conjugated secondary antibodies, and the proteins detected by SuperSignal West Femto Maximum Sensitivity Substrate (Pierce). The same blots were stripped and reprobed with desired antibodies to confirm equal loading.

Immunoprecipitation and *in vitro* kinase assay. Cell lysates from 2 μmol/L K00135–treated MV4;11 cells (60 min) were prepared as described above and incubated with either no antibodies or 2 μg of anti-PIM1/PIM2 antibody with gentle rocking at 4°C overnight. Protein A-agarose beads (Upstate; 50 μL of 50% beads slurry in 500 μL of the lysate) were added and incubated for additional 2 h, followed by 15-s microcentrifugation, three washes with 300 mmol/L lysis buffer, and two additional washes with kinase buffer [40 mmol/L Tris-HCl (pH 7.4), 20 mmol/L $MgCl_2$, 0.1 mg/mL bovine serum albumin]. Beads were then suspended in 50 μL of kinase buffer supplemented with 500 μmol/L ATP and either no inhibitor or 2 μmol/L K00135 and incubated at 30°C for 30 min. Four micrograms of soluble BAD protein (Upstate) were then added to the reaction and incubated for additional 30 min. The reactions were terminated by addition of the Laemmli sample buffer and phosphorylation of BAD was analyzed by Western blotting with anti–phospho-BAD ($Ser^{112/136}$) antibodies.

Results

Overall structure and substrate binding. The crystal structure of the ternary complex of PIM1 with a consensus substrate peptide and the inhibitor K00135 was determined at 1.9-Å resolution (Fig. 1; Supplementary Table S1) revealing the kinase with the typical bilobal architecture. The overall structure of the protein was found to be similar to structures that have previously been described (Fig. 1*A*; refs. 18–21). The serine/threonine kinase PIM1 has been shown to have a strong preference for substrates with basic residues, particularly arginine, at positions −5 and −3 (21, 22). Peptide library screening has defined additional selectivity for histidine at −2, proline at −1, and glycine at +1, facilitating the design of a high-affinity consensus peptide, pimtide (ARKRRRHPS* GPPTA). As in the case of the PIM1-BIM1 peptide complex (22), the substrate peptide was well defined between residues Lys^6 and Gly^1, whereas the termini were not visible in the electron density and assumed to be disordered.

Inhibitor binding. Although the imidazo[1,2-*b*]pyridazine inhibitor binds to the ATP binding site of PIM1, surprisingly, it does not mimic binding of ATP by forming hydrogen bonds with the kinase hinge region (shown in magenta in Fig. 1*B*), but rather binds to the opposite side of this pocket participating in a hydrogen bond network formed by the conserved active site lysine (Lys^{67}), a structural water molecule, the αC residue of Glu^{89}, and the activation loop residue Phe^{187} (Fig. 1*B*). In addition, a number of hydrophobic contacts, particularly with PIM1 residues Leu^{44}, Phe^{49}, Ile^{104}, and Leu^{120}, stabilize this interaction. The unusual hinge architecture of PIM1, which has a proline at the hinge position 123, allows formation of only one hydrogen bond to ATP or ATP mimetic inhibitors. We believe that this active site architecture, together with the unexpected binding mode of the studied imidazo[1,2-*b*]pyridazine inhibitor, results in surprisingly PIM-specific inhibitors. Indeed, the imidazo[1,2-*b*]pyridazine that cocrystallized with PIM1 interacted with only one other kinase

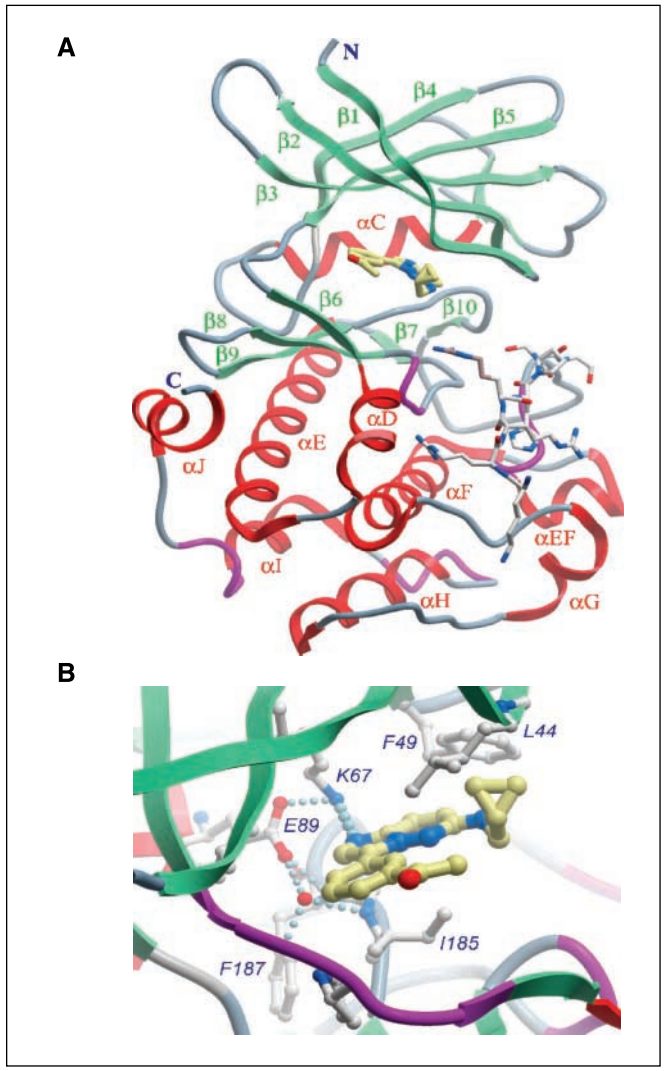

Figure 1. Structure of PIM1 in complex with the imidazopyridazine (K00135) inhibitor. *A,* structural overview: the main secondary structure elements and the NH_2 and COOH termini of the protein are labeled. The inhibitor and the substrate peptide are shown in ball-and-stick representation. *B,* a view from the hinge region (highlighted in magenta). *Dotted lines,* hydrogen bonds. Only side chains that make significant contact with the inhibitor are shown.

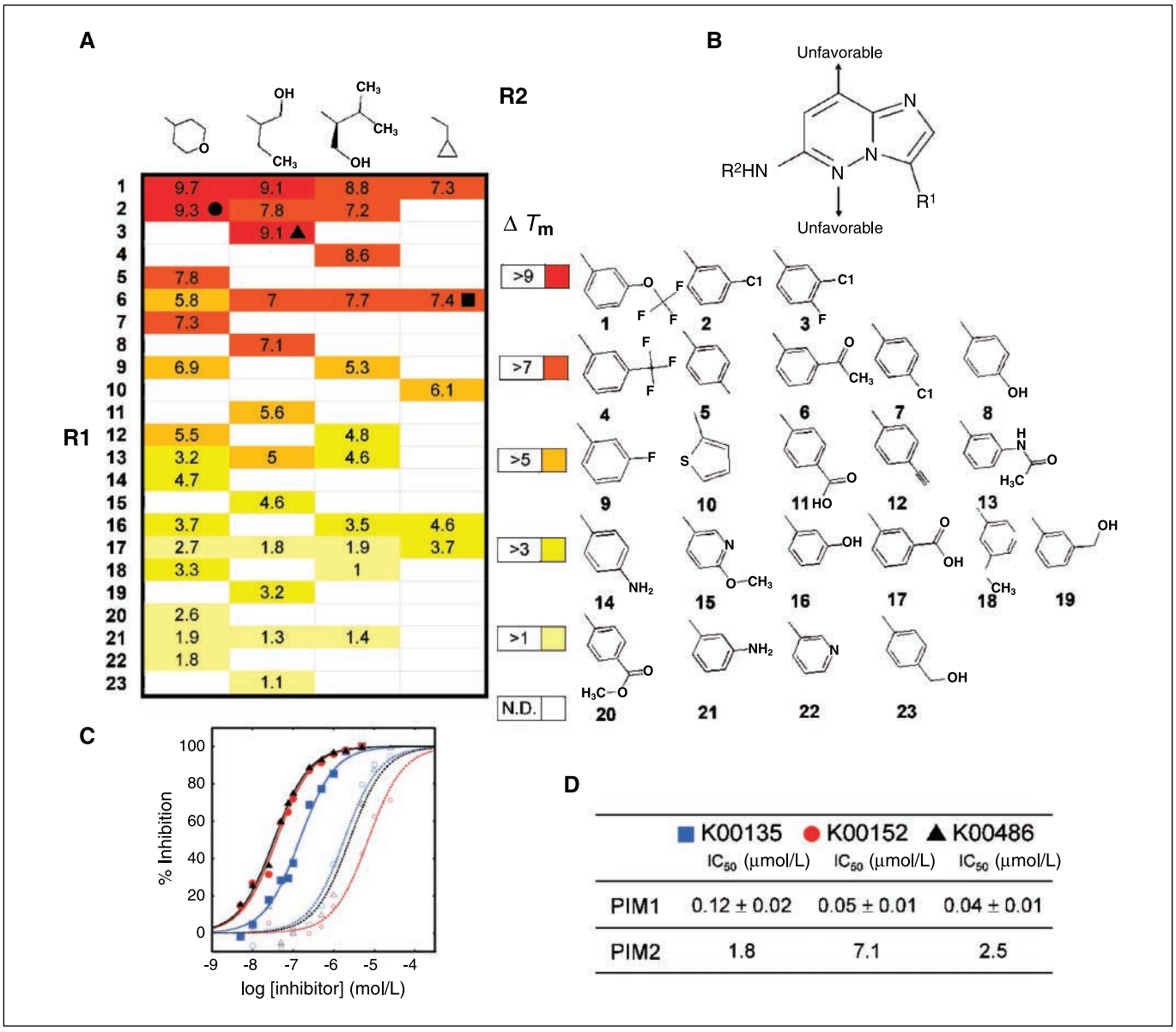

Figure 2. Structure-activity relationship of the imidazopyridazine inhibitor derivatives screened by temperature shift assays. *A,* structure-activity relationship identified on the imidazopyridazine scaffold. Shown are T_m shift data as a function of the chemical moieties in R1 and R2. The T_m shift data are color coded. The different chemical moieties studied are shown on the right side (R1) and on top (R2). Moieties present in the three inhibitors studied in cells are indicated (*triangle,* K00486; *circle,* K00152; *square,* K00135). *B,* general scaffold of the studied imidazopyridazine inhibitor showing the location of the two varied R groups. *C,* IC_{50} data determined for K00135, K00486, and K00152 on PIM1 and PIM2 (done in duplicate). Nonlinear least squares fit to the data points are shown as solid lines (PIM1) and dotted lines (PIM2). Symbols used are the same as in (*A*). *D,* table showing determined IC_{50} values for three inhibitors.

(Cdc-like kinase 1) in a panel of more than 50 diverse serine/threonine kinase catalytic domains purified for cocrystallization studies in our laboratory (Fig. 2).[5] We generated a small library of inhibitors based on the imidazo[1,2-*b*]pyridazine scaffold targeting PIM1 kinase and used temperature shift assays to identify and rank-order ligands that interact with PIM kinases. This assay monitors the linear affinity–dependent stability increase of proteins and has been shown to correlate well with binding constants and IC_{50} values (22). In the study done here, we also confirmed an excellent correlation of temperature shift data (T_m) with IC_{50} values and identified several inhibitors (K00152 and K00486) with improved potency compared with K00135 (Fig. 2*A*). The structure-activity relationship of the library was established with two varying positions (R1 and R2; Fig. 2*B*). The limited variations in position R2 did not dramatically influence T_m shift values. This is supported by the cocrystal structure, which showed that chemical moieties at that position interact with the glycine-rich loop but larger moieties would point toward the solvent. Aliphatic or saturated six-member ring systems at that position resulted in slightly more potent inhibitors than the tricyclic ring present in K00135. Within the inhibitor series tested, a trifluoromethoxy moiety in meta position of the aromatic substitution in

[5] O. Fedorov et al., in preparation.

R1 showed the highest affinity for PIM1 (Fig. 2). Our crystal structure suggests that the larger trifluoro-methoxy moiety might favorably interact with the side chain of Arg^{122}. K00135 binding was also confirmed by isothermal titration calorimetry, revealing a K_D of 25 nmol/L and a strongly enthalpy-driven interaction (not shown). It was interesting to see that, in general, PIM2 inhibition was 10- to 100-fold weaker than IC_{50} values measured for PIM1 (Fig. 2). This finding is very surprising considering the high homology between the PIM1 and PIM2 active sites. In fact, there is only one single conservative change within the ATP pocket: comparison with the PIM2 crystal structure (pdb code 1IWI) showed PIM1 Val^{126} is an alanine residue in PIM2. The close contact of Val^{126} side chain and the carbonyl oxygen of the substitution of the aromatic R2 moiety of the inhibitor is 4 Å. This interaction is not likely to contribute to the binding of the inhibitor, but an amino acid substitution at this position might influence the flexibility of the kinase hinge region. PIM3 interaction with the investigated inhibitors seems to be more similar to PIM1 (Fig. 2). Two hits identified in the screen were particularly interesting; K00486 had an IC_{50} of 34 nmol/L against PIM1 and only an IC_{50} of 2.5 μmol/L against PIM2 with an identical selectivity profile, whereas K00152 inhibited PIM1 with an IC_{50} of 39 nmol/L (PIM2 7 μmol/L) but also inhibited polo-like kinase 1 in our profiling for specificity (data not shown).

Ba/F3 cells stably expressing human PIMs. To address inhibition of PIM kinases by K00135 in a cellular system, we established a series of murine IL-3–dependent Ba/F3 cells that stably expressed human hPIM1 or hPIM2 by retroviral gene transfer. Stable expression of hPIM1 or hPIM2 allows the cells to survive in the absence of IL-3 (Fig. 3*A, top*; ref. 30). To increase the sensitivity of detection of hPIM proteins, we also generated Ba/F3 cells stably expressing NH_2-terminal FLAG-tagged human PIM kinases. No differences in cell growth were observed when tagged or untagged hPIM kinases were expressed (not shown). Interestingly, although we were able to detect high levels of hPIM mRNAs (not shown), only relatively low levels of steady-state hPIM proteins were observed (Fig. 3*A, bottom*). This is probably due to the short half-life of PIM proteins *in vivo* and their rapid proteosomal degradation. Treatment of the cells with the proteosome inhibitor MG132 led to a substantial increase in hPIM protein levels, in particular for hPIM1 (Fig. 3*A, bottom*; ref. 31). To address the effect of K00135 in Ba/F3 cells stably overexpressing hPIMs, we exposed the cells to different concentrations of K00135, ranging from nanomolar to low micromolar levels. Survival of the cells was determined after 24 h by trypan blue dye exclusion. As shown in Fig. 3*B*, a dose-dependent decrease in cell survival was observed after 24 h in Ba/F3-hPIM1 grown in the absence of IL-3. Cells expressing hPIM2 were less sensitive to K00135, as expected from the higher IC_{50} values for PIM2 determined for this compound (Fig. 2). Despite better potency in *in vitro* kinase assays, effects on cell survival using the two inhibitors K00152 and K00486 were similar (data not shown). Importantly, no significant decrease in viability was observed in wild-type Ba/F3 cells growing in IL-3 and in the presence of all three inhibitors tested. These experiments show that imidazo[1,2-*b*]pyridazines interact with and inhibit hPIM1 and, to a lesser extent, hPIM2 in a cellular system. In addition, these compounds do not seem to interfere with molecules of murine origin that are critical for IL-3–mediated cell growth.

Effect of K00135 on human leukemic cell lines. Cytotoxic effects of K00135, as well as the effect on clonogenic cell growth,

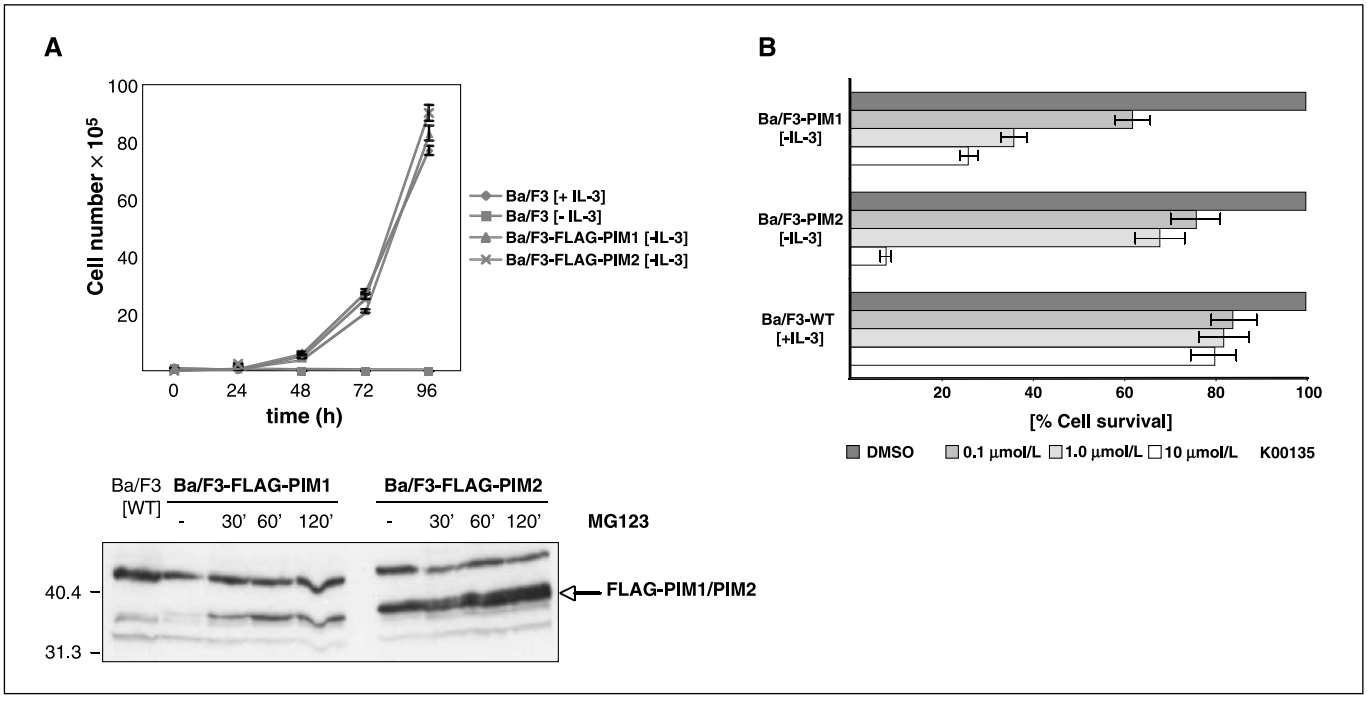

Figure 3. Effect of K00135 on Ba/F3 cells stably expressing human PIMs. *A,* stable expression of hPIM1 or hPIM2 in IL-3–dependent murine Ba/F3 cells allows the cells to survive in the absence of IL-3 (*top*). *Points,* mean from two independent experiments, each done in triplicate; *bars,* SD. FLAG-tagged PIM proteins were detected by Western blotting with anti-FLAG antibodies after treatment of cell cultures with the proteosomal inhibitor MG132 (*bottom*). *B,* same cell lines, as well as the parental Ba/F3 cells, were exposed to increasing amounts of K00135 and cell viability was determined 24 h later (expressed as a percentage normalized to viability of cells treated with 0.1% DMSO only). A dose-dependent decrease in cell survival was observed for Ba/F3-hPIM1 and, to a lesser extent, for Ba/F3-hPIM2 cells.

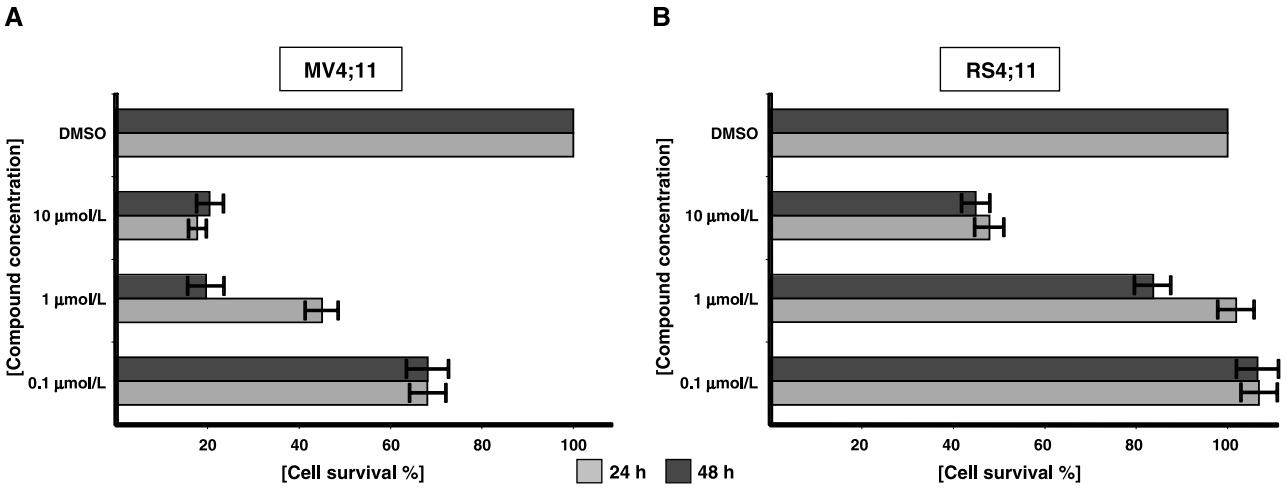

C

K00135	IC_{50} in μmol/L (48 h)
MV4;11	0.4
RS4;11	8.8
MOLM13	0.3
KOCL45	8.2
SEM	6
KOPN8	6.1
K562	8

Figure 4. Effect of K00135 on human leukemia cell lines. Increasing amounts of K00135 were added to MV4;11 (*A*) or RS4;11 (*B*) and other cell lines, and cell viability (as in Fig. 3*B*) and IC_{50} values were determined 24 and 48 h later (*C*).

were tested in a series of human leukemia cell lines (MV4;11, RS4;11, MOLM13, KOCL45, SEM, KOPN8, and K562). As shown in Fig. 4, some cytotoxic effects of K00135 were observed in all cell lines tested. Interestingly, cell lines that harbor the FLT3-ITD mutation, such as MV4;11 or MOLM13, were up to 20 times more sensitive than K562 cells that originate from BCR/ABL–positive blast crisis patient (Fig. 4*C*). We also assessed the effect of K00135 on clonogenic growth of leukemic cells. Among the cell lines included in our study, only MV4;11, MOLM13, and K562 were able to form colonies (>50 cells) when plated in methylcellulose (not shown). A significant reduction in clonogenic growth was observed in MV4;11 and MOLM13 even at an inhibitor concentration of <1 μmol/L, whereas colony formation of K562 was not affected even at a higher dose as expected from the relative resistance of this cell line to the treatment with this inhibitor class (Supplementary Fig. S1*A*).

K00135 induces apoptosis in human leukemic cell line MV4;11. K00135 induced cytotoxicity in both hPIM1/hPIM2–overexpressing Ba/F3 cells and all leukemic cell lines tested. To determine the mechanism of K00135-mediated cell death, we measured by flow cytometry the induction of apoptosis in MV4;11 cells treated with 1 μmol/L K00135 at different time points after inhibitor exposure. We used both dye PO-PRO-1, which is a sensitive indicator of apoptotic cells, and 7-amino-actinomycin D, an indicator of dead cells. The percentage of apoptotic MV4;11 cells increased in a time-dependent manner, with 2.8% of the cells undergoing apoptosis and 15.3% dead after 12 h and 8.5% apoptotic and 40.5% dead cells after 36 h of treatment (Supplementary Fig. S1*B*).

K00135 impairs phosphorylation of PIM downstream targets. To show that PIM kinases are indeed targeted by K00135 in leukemic cells, we monitored the *in vitro* kinase activity of immunoprecipitated PIM on its downstream targets by Western blotting with phospho-specific antibodies. The antiapoptotic protein BAD has been shown to be directly serine phosphorylated by both PIM1 and PIM2 (32, 33). To show inhibition of PIM activity in MV4;11 cells, PIM protein was immunoprecipitated and analyzed for its ability to phosphorylate BAD (on Ser^{112} and Ser^{136}) *in vitro* in the presence (1 h) or absence of K00135 (2 μmol/L). As shown in Fig. 5*A*, phosphorylation of BAD by PIM1 and PIM2 was abrogated on addition of the compound. To further analyze the effects of K00135 on PIM function, phosphorylation of two known direct PIM targets (BAD and 4E-BP1) was followed by immunoblotting. As shown in Fig. 5*B*, short-term exposure of the cells to 1 μmol/L K00135 led to a significant decrease of phosphorylation of BAD and 4E-BP1. In contrast, no changes in phosphorylation of FLT3-ITD or Akt/protein kinase B were observed (data not shown). These results suggest that K00135 exerts its effects in MV4;11 by interfering primarily with PIM kinases downstream of FLT3-ITD or Akt/protein kinase B.

K00135 impairs *in vitro* survival of primary leukemic blasts. Next, we analyzed the effects of K00135 on the growth of leukemic blasts from five patients with newly diagnosed AML. When cultured in methylcellulose, the cells from AML patients grew in small clusters (Fig. 6*B*) and were therefore not amendable to be analyzed by classic quantitative colony forming assays. However, as shown in Fig. 6*A*, exposure of leukemic blasts in a short-term liquid culture to K00135 resulted in a significant decrease in survival for all patient samples. Although K00135 showed an effect on colony formation of all primary cells analyzed, no significant difference in survival between the patients harboring FLT3-ITD (patients 1 and 2) or those without (patients 3–5) was observed.

Finally, we have addressed the cytotoxic effects of K00135 on normal human cord blood cells at antileukemic doses. As shown in Fig. 6*C*, K00135, at concentrations of 1 to 10 μmol/L, had only a minor effect on survival of normal umbilical blood mononuclear cells from four healthy donors.

Discussion

Recent reports showing that PIM kinases are involved in malignant transformation of hematopoietic cells by oncogenic tyrosine kinases provided a strong rationale for development of PIM kinase inhibitors as potential therapeutics (11–17). All PIM inhibitor structures that have been published to date interact with the kinase hinge region in a classic ATP mimetic way. Screening of a kinase-targeted library and structure-activity relationship analysis allowed us to identify several imidazo[1,2]pyridazines with high affinity for PIM1. Related inhibitors of the pyrazolpyrimidine class were first described as specific inhibitors of the Src family of tyrosine kinases, with several pyrazolo[3,4-*d*]pyrimidines having low nanomolar affinity for Lck and anticancer activity (34). One of these compounds, PP1, was later crystallized in complex with the autoinhibited form of Hck, providing further guidance for drug development (35). Subsequently, this scaffold yielded specific inhibitors for glycogen synthase kinase 3 and members of the cyclin-dependent kinase (CDK) family (36). Inhibitors based on the variant pyrazolo[1,5-*a*]pyrimidine scaffold have also been described with specificity for CDK2 and the KDR kinase domain (37–39). However, all published cocrystal structures of this inhibitor class show binding to the kinase hinge region in the expected type I binding mode. Here, we identified a binding mode for our compound in which the inhibitor interacts with the opposite side of the ATP binding pocket, without making significant polar contacts with the kinase hinge region. In addition, the DFG motif did not move into an "out" conformation as observed in cocrystal structures of kinases with type II inhibitor complexes. However, the described area of the binding pocket is much more diverse than the hinge region, bearing the promise that

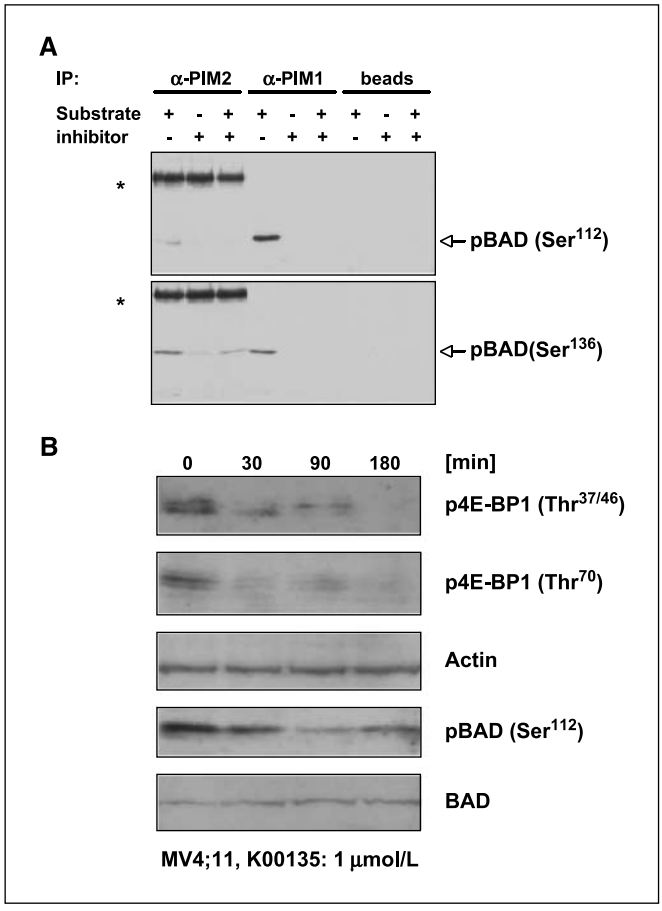

Figure 5. K00135 impairs phosphorylation of downstream targets of PIM. *A,* PIM proteins were immunoprecipitated from MV4;11 cells and the agarose-protein A-immunoprecipitate complex was tested for its ability to phosphorylate BAD *in vitro* in the presence or absence of K00135. Phosphorylation of BAD (both on Ser^{112} and Ser^{136}, detected by Western blotting with phospho-specific antibodies) was abrogated on addition of the compound. *Asterisks,* strong bands corresponding to the heavy chain of the anti-PIM2 rabbit antibody recognized by the antirabbit immunoglobulin G secondary antibody. Beads alone (without anti-PIM antibodies) were incubated with the MV4;11 extract and used for the same *in vitro* phosphorylation reaction as a negative control. *B,* MV4;11 cells were incubated with 1 μmol/L K00135 for indicated times, harvested, and protein extracts separated by SDS-PAGE. The effect of K00135 on PIM endogenous targets was followed by Western blotting with indicated phospho-specific antibodies. Membranes were stripped and reprobed with anti-actin and anti-BAD (total) antibodies to check for equal loading.

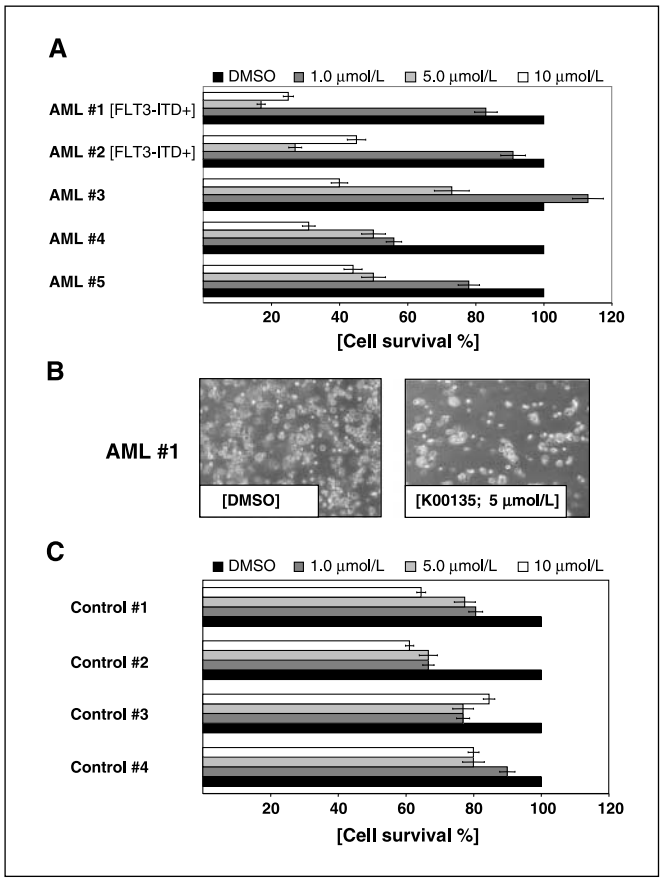

Figure 6. K00135 impairs *in vitro* survival of primary leukemic blasts. *A,* leukemic blasts from five patients were grown in liquid cultures without the drug or with increasing amounts of K00135, and cell viability was determined 24 h later (expressed as a percentage normalized to viability of cells treated with 0.1% DMSO only). *B,* when cultured in methylcellulose in the presence of K00135, significantly lower density of characteristic small leukemic clusters was observed as compared with control cultures (shown only for one patient sample; *right*). *C,* cytotoxic effects of K00135 (at antileukemic doses) were analyzed in liquid cultures of umbilical vein–derived mononuclear cells from four healthy donors, and cell viability was determined as percentage compared with viability of cells treated with DMSO only. *Columns,* mean of two independent experiments, each done in triplicate; *bars,* SD.

more specific inhibitors may be developed on the basis of the determined crystal structure. Indeed, we observed cross-reactivity with only one other kinase (Cdc-like kinase 1) within a panel of 50 serine-threonine kinases currently present in our laboratory.[6]

Several compounds that inhibit PIM1 *in vitro* with nanomolar potency were selected for *in vivo* profiling using murine Ba/F3 cells overexpressing human PIM1 or PIM2 (30). Three compounds showed a dose-dependent inhibition of cell survival in hPIM-expressing Ba/F3 cells, but not in wild-type cells growing in the presence of IL-3 (Fig. 3). This suggests that PIM activity may not be essential for growth and survival of murine Ba/F3 cells signaling through IL-3, or simply that the compounds can interact and inhibit only human but not mouse PIM kinases. Additional experiments carried out with IL-3–independent Ba/F3 cells overexpressing mouse PIMs strongly suggest the latter possibility (data not shown).

The nanomolar *in vitro* potencies of the selected inhibitors using purified PIM protein translated into low micromolar potencies in the Ba/F3 cell model. The compounds were further tested in several human leukemia cell lines. Some AML cell lines such as MV4;11 or MOLM13 were very sensitive to the selected PIM1 inhibitors with IC_{50} values well below 1 μmol/L in cell survival studies; however, other cell lines, such as K562 (chronic myelogenous leukemia blast crisis), were less affected (Fig. 4*C*). The molecular correlates that determine the sensitivity of PIM inhibitors are currently unknown, but preliminary results suggest that effects on cell survival may not fully correlate with PIM kinase expression levels (data not shown). In addition to cytotoxic effects, the tested inhibitors also significantly reduced the self-renewal capacity of leukemic cells as shown by inhibition of their clonogenic activity. Interestingly, there are several lines of evidence suggesting that PIM1 may functionally cooperate with Gfi1, a known regulator of self-renewal of hematopoietic stem cells (40). In addition, the homeobox transcription factor HOXa9, another regulator of self-renewal capacity and frequently deregulated in human acute leukemia, seems to regulate expression of PIM1 in hematopoietic stem cells, further supporting PIM1 as a therapeutic target for this disease (41).

Indeed, exposure of blasts from five AML patients to our PIM1 kinase inhibitors leads to a significant reduction in cell survival after 24 h (Fig. 6*A*). Interestingly, exposure of mononuclear cells from human cord blood from four donors to the compounds was associated with minimal cytotoxic effects (Fig. 6*C*). Mice lacking all known PIMs (PIM1, PIM2, and PIM3) are fertile and have a normal life span, suggesting that PIMs may not be essential for steady-state homeostasis, although deregulated on malignant transformation (42). Biochemical analysis strongly suggests that our compounds indeed block PIM1 function and its downstream targets such as BAD or 4E-BP1. However, a drawback of the identified compounds may be that significant reduction of growth and survival of human leukemia cell lines or primary samples could only be achieved at relatively high (micromolar) compound concentrations. Further experiments are necessary to determine whether micromolar serum level can be achieved in a living organism. Additional modification of the molecule core may further increase the affinity of the compounds. Strategies to modify PIM expression and/or stabilization may also be explored for the treatment of hematopoietic malignancies, and possible additive effects of combinations of PIM kinase inhibitors with heat shock protein-90 inhibitors such as 17-*N*-allylamino-17-demethoxygeldanamycin derivatives are currently investigated (31, 43). One should also keep in mind that PIM kinases have been intensively characterized as proteins of relatively weak inherent oncogenicity but potent in cooperation with other oncogenes such as *c-myc* (44–47). Therefore, it is likely that synergistic effects may be achieved in combination with either traditional chemotherapeutics and/or other small molecules that target signaling cascades linked to survival of the malignant cells.

K00135 shows selectivity for PIM1. Although previous studies have shown that an optimal PIM-targeted tumor therapy would include inhibition of PIM2 (12, 15, 17), thus far, there is no potent inhibitor for PIM2 available. Interestingly, all reported inhibitors show selectivity for PIM1, suggesting that PIM2 is intrinsically more difficult to target. This finding is surprising considering the high sequence conservation of the PIM1 and PIM2 active sites. It is therefore likely that dynamic variables that are currently not understood may also play a role in the recognition process. Strong research efforts are currently put into a search for PIM1 and PIM2 inhibitors.

This is the first report of a class of compounds that inhibit PIM kinases with clear anticancer activity as shown in leukemic cell lines as well as primary blasts from AML patients. Deregulated expression of PIM1 in other hematologic tumors (high grade lymphoma) and solid tumors, such as prostate carcinoma or oral squamous cell cancer, suggests that efficient inhibition of these kinases by small molecules may lead to potent targeted cancer therapy (48–50).

Acknowledgments

Received 1/24/2007; revised 4/5/2007; accepted 5/3/2007.

Grant support: Gertrude von Meissner Foundation, the Swiss National Science Foundation and ONCOSUISSE (J. Schwaller). The Structural Genomics Consortium is a registered charity (no. 1097737) funded by the Wellcome Trust, GlaxoSmithKline, Genome Canada, the Canadian Institutes of Health Research, the Ontario Innovation Trust, the Ontario Research and Development Challenge Fund, the Canadian Foundation for Innovation, VINNOVA, The Knut and Alice Wallenberg Foundation, The Swedish Foundation for Strategic Research, and Karolinska Institutet.

The costs of publication of this article were defrayed in part by the payment of page charges. This article must therefore be hereby marked *advertisement* in accordance with 18 U.S.C. Section 1734 solely to indicate this fact.

We thank Sabine Ehret, Michael Sundström, and other members of our laboratories for their input in this work.

[6] http://www.sgc.ox.ac.uk

References

1. Chalandon Y, Schwaller J. Targeting mutated protein tyrosine kinases and their signaling pathways in hematologic malignancies. Haematologica 2005;90:949–68.
2. De Keersmaecker K, Cools J. Chronic myeloproliferative disorders: a tyrosine kinase tale. Leukemia 2006;20:200–5.
3. Giles FJ, Cortes JE, Kantarjian HM. Targeting the kinase activity of the BCR-ABL fusion protein in patients with chronic myeloid leukemia. Curr Mol Med 2005;5:615–23.
4. O'Hare T, Corbin AS, Druker BJ. Targeted CML therapy: controlling drug resistance, seeking cure. Curr Opin Genet Dev 2006;16:92–9.
5. Cuypers HT, Selten G, Quint W, et al. Murine leukemia virus-induced T-cell lymphomagenesis: integration of proviruses in a distinct chromosomal region. Cell 1984;37:141–50.
6. Mikkers H, Allen J, Knipscheer P, et al. High-throughput retroviral tagging to identify components of specific signaling pathways in cancer. Nat Genet 2002;32:153–9.
7. Mui AL, Wakao H, Kinoshita T, Kitamura T, Miyajima

A. Suppression of interleukin-3-induced gene expression by a C-terminal truncated Stat5: role of Stat5 in proliferation. EMBO J 1996;15:2425–33.
8. Nosaka T, Kawashima T, Misawa K, Ikuta K, Mui AL, Kitamura T. STAT5 as a molecular regulator of proliferation, differentiation and apoptosis in hematopoietic cells. EMBO J 1999;18:4754–65.
9. Schwaller J, Parganas E, Wang D, et al. Stat5 is essential for the myelo- and lymphoproliferative disease induced by TEL/JAK2. Mol Cell 2000;6:693–704.
10. Sternberg DW, Gilliland DG. The role of signal transducer and activator of transcription factors in leukemogenesis. J Clin Oncol 2004;22:361–71.
11. Amson R, Sigaux F, Przedborski S, Flandrin G, Givol D, Telerman A. The human proto-oncogene product p33pim is expressed during fetal hematopoiesis and in diverse leukemias. Proc Natl Acad Sci U S A 1989;86: 8857–61.
12. Mizuki M, Schwable J, Steur C, et al. Suppression of myeloid transcription factors and induction of STAT response genes by AML-specific Flt3 mutations. Blood 2003;101:3164–73. Epub 2002 Dec 05.
13. Cohen AM, Grinblat B, Bessler H, et al. Increased expression of the hPim-2 gene in human chronic lymphocytic leukemia and non-Hodgkin lymphoma. Leuk Lymphoma 2004;45:951–5.
14. Nieborowska-Skorska M, Hoser G, Kossev P, Wasik MA, Skorski T. Complementary functions of the antiapoptotic protein A1 and serine/threonine kinase pim-1 in the BCR/ABL-mediated leukemogenesis. Blood 2002;99:4531–9.
15. Hammerman PS, Fox CJ, Birnbaum MJ, Thompson CB. Pim and Akt oncogenes are independent regulators of hematopoietic cell growth and survival. Blood 2005; 105:4477–83.
16. Kim KT, Baird K, Ahn JY, et al. Pim-1 is up-regulated by constitutively activated FLT3 and plays a role in FLT3-mediated cell survival. Blood 2005;105:1759–67.
17. Adam M, Pogacic V, Bendit M, et al. Targeting PIM kinases impairs survival of hematopoietic cells transformed by kinase inhibitor-sensitive and kinase inhibitor-resistant forms of Fms-like tyrosine kinase 3 and BCR/ABL. Cancer Res 2006;66:3828–35.
18. Qian KC, Wang L, Hickey ER, et al. Structural basis of constitutive activity and a unique nucleotide binding mode of human Pim-1 kinase. J Biol Chem 2005;280: 6130–7.
19. Kumar A, Mandiyan V, Suzuki Y, et al. Crystal structures of proto-oncogene kinase Pim1: a target of aberrant somatic hypermutations in diffuse large cell lymphoma. J Mol Biol 2005;348:183–93.
20. Jacobs MD, Black J, Futer O, et al. Pim-1 ligand-bound structures reveal the mechanism of serine/threonine kinase inhibition by LY294002. J Biol Chem 2005;280:13728–34.
21. Bullock AN, Debreczeni J, Amos AL, Knapp S, Turk BE. Structure and substrate specificity of the Pim-1 kinase. J Biol Chem 2005;280:41675–82.
22. Bullock AN, Debreczeni JE, Fedorov OY, Nelson A, Marsden BD, Knapp S. Structural basis of inhibitor specificity of the human proto-oncogene proviral insertion site in Moloney murine leukemia virus (PIM-1) kinase. J Med Chem 2005;48:7604–14.
23. Cook PF, Neville ME, Jr., Vrana KE, Hartl FT, Roskoski R, Jr. Adenosine cyclic 3′,5′-monophosphate dependent protein kinase: kinetic mechanism for the bovine skeletal muscle catalytic subunit. Biochemistry 1982;21: 5794–9.
24. Matulis D, Kranz JK, Salemme FR, Todd MJ. Thermodynamic stability of carbonic anhydrase: measurements of binding affinity and stoichiometry using ThermoFluor. Biochemistry 2005;44:5258–66.
25. Leslie AGW. Joint CCP4 and ESF-EAMCB Newsletter on Protein Crystallography, No. 26; 1992.
26. Evans PR. Data reduction. In: Proceedings of CCP4 Study Weekend on Data Collection and Processing 1993. Warrington (UK): Daresbury Laboratory; 1993. p. 114–122.
27. Storoni LC, McCoy AJ, Read RJ. Likelihood-enhanced fast rotation functions. Acta Crystallogr D Biol Crystallogr 2004;60:432–8.
28. Murshudov GN, Vagin AA, Dodson EJ. Refinement of macromolecular structures by the maximum-likelihood method. Acta Crystallogr D Biol Crystallogr 1997;53:240–55.
29. McRee DE. XtalView/Xfit-A versatile program for manipulating atomic coordinates and electron density. J Struct Biol 1999;125:156–65.
30. Nosaka T, Kitamura T. Pim-1 expression is sufficient to induce cytokine independence in murine hematopoietic cells, but is dispensable for BCR-ABL-mediated transformation. Exp Hematol 2002;30:697–702.
31. Shay KP, Wang Z, Xing PX, McKenzie IF, Magnuson NS. Pim-1 kinase stability is regulated by heat shock proteins and the ubiquitin-proteasome pathway. Mol Cancer Res 2005;3:170–81.
32. Macdonald A, Campbell DG, Toth R, McLauchlan H, Hastie CJ, Arthur JS. Pim kinases phosphorylate multiple sites on Bad and promote 14-3-3 binding and dissociation from Bcl-XL. BMC Cell Biol 2006;7:1.
33. Kim KT, Levis M, Small D. Constitutively activated FLT3 phosphorylates BAD partially through pim-1. Br J Haematol 2006;134:500–9.
34. Hanke JH, Gardner JP, Dow RL, et al. Discovery of a novel, potent, and Src family-selective tyrosine kinase inhibitor. Study of Lck- and FynT-dependent T cell activation. J Biol Chem 1996;271:695–701.
35. Schindler T, Sicheri F, Pico A, Gazit A, Levitzki A, Kuriyan J. Crystal structure of Hck in complex with a Src family-selective tyrosine kinase inhibitor. Mol Cell 1999; 3:639–48.
36. Markwalder JA, Arnone MR, Benfield PA, et al. Synthesis and biological evaluation of 1-aryl-4,5-dihydro-1*H*-pyrazolo[3,4-*d*]pyrimidin-4-one inhibitors of cyclin-dependent kinases. J Med Chem 2004;47:5894–911.
37. Moravcova D, Krystof V, Havlicek L, Moravec J, Lenobel R, Strnad M. Pyrazolo[4,3-*d*]pyrimidines as new generation of cyclin-dependent kinase inhibitors. Bioorg Med Chem Lett 2003;13:2989–92.
38. Williamson DS, Parratt MJ, Bower JF, et al. Structure-guided design of pyrazolo[1,5-*a*]pyrimidines as inhibitors of human cyclin-dependent kinase 2. Bioorg Med Chem Lett 2005;15:863–7.
39. Fraley ME, Hoffman WF, Rubino RS, et al. Synthesis and initial SAR studies of 3,6-disubstituted pyrazolo[1,5-*a*]pyrimidines: a new class of KDR kinase inhibitors. Bioorg Med Chem Lett 2002;12:2767–70.
40. Schmidt T, Karsunky H, Gau E, Zevnik B, Elsasser HP, Moroy T. Zinc finger protein GFI-1 has low oncogenic potential but cooperates strongly with pim and myc genes in T-cell lymphomagenesis. Oncogene 1998;17: 2661–7.
41. Hu JL, Passegue E, Fong S, Largman C, Lawrence HJ. Evidence that the Pim1 kinase gene is a direct target of HOXA9. Blood 2007;109:4732–8.
42. Mikkers H, Nawijn M, Allen J, et al. Mice deficient for all PIM kinases display reduced body size and impaired responses to hematopoietic growth factors. Mol Cell Biol 2004;24:6104–15.
43. Mizuno K, Shirogane T, Shinohara A, Iwamatsu A, Hibi M, Hirano T. Regulation of Pim-1 by Hsp90. Biochem Biophys Res Commun 2001;281:663–9.
44. Shirogane T, Fukada T, Muller JM, Shima DT, Hibi M, Hirano T. Synergistic roles for Pim-1 and c-Myc in STAT3-mediated cell cycle progression and antiapoptosis. Immunity 1999;11:709–19.
45. Feldman BJ, Reid TR, Cleary ML. Pim1 cooperates with E2a-Pbx1 to facilitate the progression of thymic lymphomas in transgenic mice. Oncogene 1997;15: 2735–42.
46. Moroy T, Grzeschiczek A, Petzold S, Hartmann KU. Expression of a Pim-1 transgene accelerates lymphoproliferation and inhibits apoptosis in lpr/lpr mice. Proc Natl Acad Sci U S A 1993;90:10734–8.
47. van Lohuizen M, Verbeek S, Krimpenfort P, et al. Predisposition to lymphomagenesis in pim-1 transgenic mice: cooperation with c-myc and N-myc in murine leukemia virus-induced tumors. Cell 1989;56: 673–82.
48. Pasqualucci L, Neumeister P, Goossens T, et al. Hypermutation of multiple proto-oncogenes in B-cell diffuse large-cell lymphomas. Nature 2001;412:341–6.
49. Dhanasekaran SM, Barrette TR, Ghosh D, et al. Delineation of prognostic biomarkers in prostate cancer. Nature 2001;412:822–6.
50. Chiang WF, Yen CY, Lin CN, et al. Up-regulation of a serine-threonine kinase proto-oncogene Pim-1 in oral squamous cell carcinoma. Int J Oral Maxillofac Surg 2006;35:740–5.